5 DENSITY MODEL

The aim of this work was to develop a 3D density model of the study area, which would be consistent with the recent knowledge and geological/geophysical results described in previous chapters.
The density model was constructed using the IGMAS software.

5.1 IGMAS

5.1.1 Mathematical background

IGMAS (Interactive Gravity and Magnetics Application System) is a tool applied for the interpretation of measured gravity and magnetic fields. It is an indirect modelling approach using trial-and-error forward modelling. It works by means of a numerical simulation of underground structures that are described as closed polyhedrons of constant density/susceptibility, whose surface is triangulated (Götze 1976, 1978, 1984; Götze & Lahmeyer, 1988; Schmidt and Götze 1998, 1999). The volume integral (formula 5.1.1) is first transformed into a surface integral by means of the Gauss and Green integral theorems, and then into a line integral (formula 5.1.5). Using this algorithm, the potential field calculations are performed. For the gravity effect, for instance, one writes:

$$U(P)=G\iiint_{poly}(\frac{1}{R})\,dm \quad (5.1.1)$$

where U is the gravity potential, G is the gravitational constant and R is the distance between a point P and the volume element dm.

Considering that dm =ρ×dv, the following formula for the vertical component of the potential U ($\mathbf{g}_z$(P)), (formula 5.1.3), can be written:

$$\frac{\partial U}{\partial z}(P)=\boldsymbol{g}_z(P)=G\rho\iiint_{poly}\frac{\partial}{\partial z}(\frac{1}{R})dv \quad (5.1.2)$$

because $\boldsymbol{g}=(\frac{\partial U}{\partial x},\frac{\partial U}{\partial y},\frac{\partial U}{\partial z},)^T$ (5.1.3)

Using the Gauss theorem (Götze, 1976), which transforms a volume integral into a surface integral, one obtains:

$$\frac{\partial U}{\partial z}(P)=\boldsymbol{g}_z(P)=G\rho\oiint_{Surface}\cos(\boldsymbol{n},z)(\frac{1}{R})dS \quad (5.1.4)$$

This relationship can be also expressed as:

$$\frac{\partial U}{\partial z}(P)=\boldsymbol{g}_z(P)=G\rho\sum_{j=1}^{m}\left\{\cos(\boldsymbol{n}_{jo}z)\iint_S(\frac{1}{R})dS_j\right\} \quad (5.1.5)$$

where S_j (j=1,2,.....m) are the polyhedron surfaces, $\mathbf{n}_j$ is a surface normal of S_j and cos($\mathbf{n}_j$,z) determines the the direction of the surface element dS with respect to the Cartesian coordinate system.

The formula (5.1.5) holds true because the cos($\mathbf{n}_j$,z) is constant for any polyhedron surface. Therefore, the attraction effect of a polyhedron can be expressed as a superposition of the gravity effects of its individual surfaces S_j (Götze & Lahmeyer, 1988).

Dividing a polyhedron into separate surfaces (e.g. triangles, as is the case for IGMAS), the gravitational effect of a polyhedron is calculated after expression:

$$\mathbf{g}(P)=G\rho(\sum_{j=1}^{m}\cos(\mathbf{n}_j,z)\{\sum_{i=1}^{K_j}d_{j,i}\ln\left[\frac{b_{j.i}+\overline{PV}_{j,i-1}}{a_{j,i}+\overline{PV}_{j,i}}+\frac{\left|\overline{PP}_{j^*}\right|}{d_{j,i}}(\arctan\frac{r_{j,i-1}+b_{j.i}+\overline{PV}_{j,i-1}}{\left|\overline{PP}_{j^*}\right|\left|d_{j,i}\right|}-\right.$$

$$\left.-\arctan\frac{(r_{j,i})^2+a_{j,i}\overline{PV}_{j,i-1}}{\left|\overline{PP}_{j^*}\right|\left|d_{j,i}\right|})\right]+2\pi\left|\overline{PP}_{j^*}\right|\delta\varepsilon\}) \quad (5.1.6)$$

where P_j^* is the orthogonal projection of the station P, $V_{j,i}$ are the vertices of surfaces (e.g.triangles) and m is the number of surfaces.

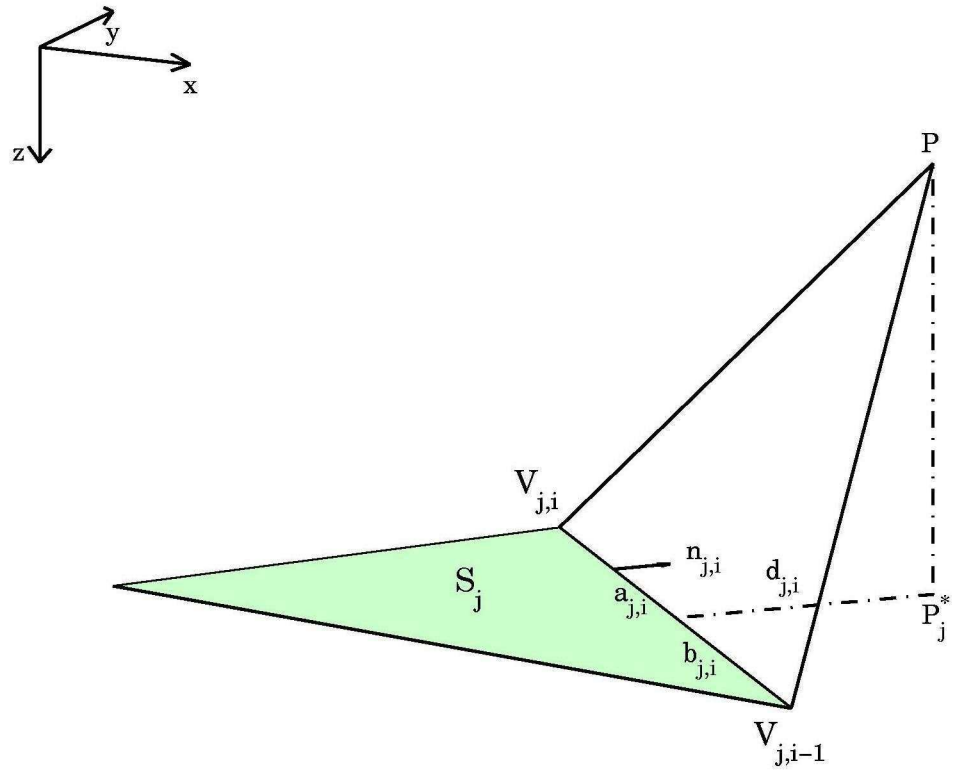

Figure 5.1
Diagram illustrating the terms used in formula 5.1.6. The surface shown here is a triangle, with its surface S_j, the vertices $V_{j,i}$, the orthogonal projection P_j^* of a station (point P), and a linear normal vector $n_{j,i}$.

5.1.2 Three dimensional structure

The interpretation of a potential field (gravity or magnetic) in the IGMAS system is based on determining shapes, positions, and physical parameters of the geological structures that cause that particular field in an investigation area. The problem of data inversion requires the application of information that has been obtained by various measurements (geological, geophysical, geodetical, petrological etc.). The indirect modelling approach includes calculation of the effect of modelled bodies that approximate geological structures in a study area, followed by matching the modelled curve with the observed gravity curve. The modelled bodies are adjusted by trial and error method using interactive graphical tools until a good fit is obtained. 3D structure is achieved in IGMAS by including several vertical

planes (Figure 5.2), on which geological bodies are geometrically defined in the form of polygons that are based on all the available data (e.g. geographical maps for the horizontal location of vertices constituting the polygons related to the modelled geological structures, together with the depth information, e.g. bathymetry for the ocean floor and a trench; and other additional data described below). The planes are always parallel and should be placed perpendicular to the geological structures that they represent. Through triangulation, these cross sections with defined polygons are connected to create the layer boundaries (triangular facets). These triangular facets represent the shape and form of the modelled geological structures of constant density or susceptibility. The triangulation between the vertical planes is performed automatically. The construction of the final three-dimensional modelled structures is done by the IGMAS system and does not require any knowledge of the topology of a model and/or the triangulation techniques (Schmidt, 1996). All the processes are done visually and interactively.

The computed gravity effect of the given structures is compared with the measured field and geometries and/or a certain physical parameter are changed until a suitable fit is achieved.

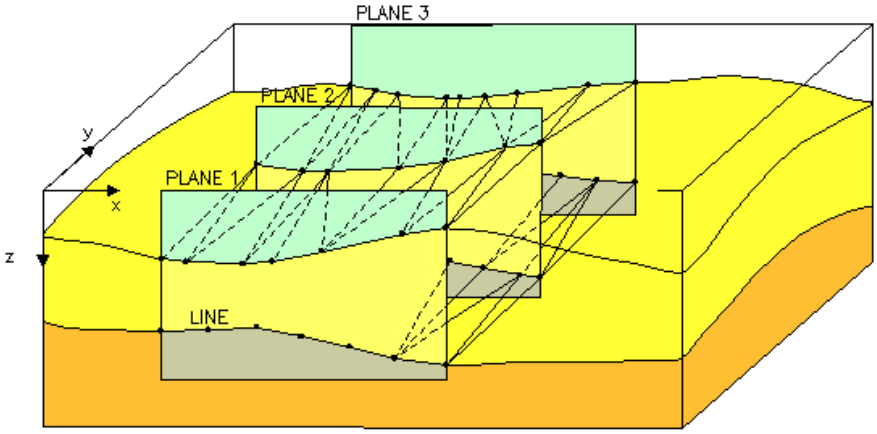

Figure 5.2
3D structure in IGMAS. It is built, in this example by three 2D vertical planes (the minimum requirement are two vertical cross sections), that are connected by triangulation between common interfaces. The data structure in IGMAS, which is required for the description of three dimensional model geometry must be simple and flexible enough to visualize the results obtained. Therefore, it includes representations of geological information, such as vertical or horizontal cross sections, surface and depth contour maps, 3D visualization, as well as volume and mass calculations.

5.1.3 Constraining data and GIS functions

The problem of forward (and also backward) modelling methods, which deal with quantitative modelling of measured geophysical fields, is the integration of additional information into the modelling process. Correct interpretation in geophysics requires an interdisciplinary knowledge, integration and consideration of 'state of the art' information from comprehensive databases. Towards this end a combination of different geophysical surveys employing seismics, gravity, magnetics, and geoelectrics, together with geological, mineralogical, petrological studies, and results from remote sensing, provides new insights into the structures and tectonic evolution of natural deposits and crustal structure. The interdisciplinary approach is essential for numerical modelling of these structures and the processes acting on them. In most of geophysical data interpretation, various geophysical methods are used to yield an increased number of models. Some of these models are in 3D, but most of them are still in 2D and some even in 1D. These data are usually inhomogeneous, arbitrarily distributed, and in some cases they might also be uncertain, especially if they describe human interpretation of certain observations. Some examples of information, which are of specific interest for gravity and magnetic modelling are listed below.

Geological data, e.g**:**

- Geological maps
- Location and course of fault zones
- Density determinations of rock samples and cores.

Results from other geophysical methods , e.g:

- Location of hypocentres
- Refraction seismic profiles
- Reflection seismics, line drawings
- Receiver function studies
- Electrical conductivity, deduced from geoelectrics and magnetotellurics
- Tomography models

(Schmidt, 1996).

The modelling approach applied to complex interpretation tools requires a synoptical visualization of the necessary constraining data, which have to be selected and activated by a user. This task is performed by GeoInformationSystems (GIS) that are usually based on relational data banks, or object orientated systems (OOS). The advantage of OOS is an increasing effect due to direct access to data and information through definition of 'geo-objects'

(Breunig et al., 1999; Breunig et al., 2000; Schmidt & Götze, 1998; Schmidt & Götze, 1999).

In IGMAS, constraints are visualized on the computer screen to directly provide the information of the available data sets to a user. They are shown as overlays on the model geometry (Figures 5.3 and 5.4), and may be activated or deactivated interactively to avoid confusing display of multiple datasets. Visualization functions used by IGMAS (e.g. arbitrarily located cross sections and maps) require either a projection of the constraining data on the actual cross section, or a slice through the data along the selected plane. The additional data may be 1D, 2D or even 3D.

Point data, e.g. hypo- or epicentres (Figure 5.3), volcanoes and borehole measurement require two (x, y) or three (x, y, z) coordinates and sometimes additional attributes like magnitude, age etc. If the z-coordinate is not given, points are projected to the surface of the model. The projection strip may be defined by the user so that points beyond projection plane are ignored. (More examples are shown in Figures 6.1–6.4, Section 6.1).

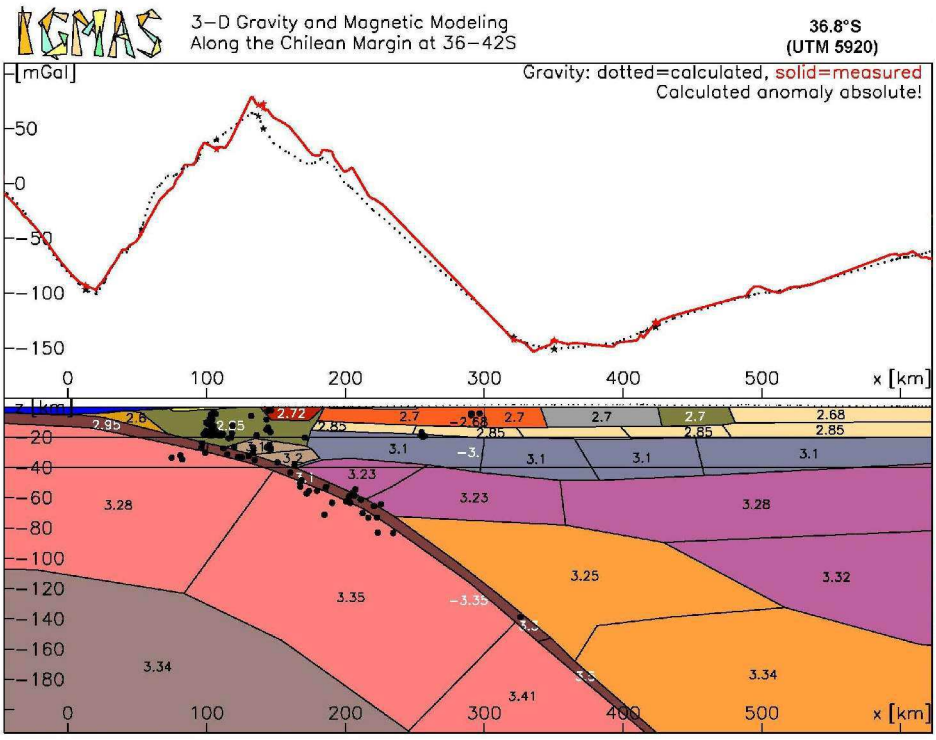

Figure 5.3

An example of a 2D cross-section from the density model at 36.8°S with earthquake hypocentres from the ISSA catalogue (Bohm et al., 2002).

Two-dimensional information (lines and profiles), e.g. geological sections or maps, seismic models (Figure 5.4), local earthquake tomography model cross sections and receiver function models. These data require two (x, y) or three (x, y, z) coordinates. If z- coordinates are not given (e.g. for political border lines), they are projected to the surface of the model.

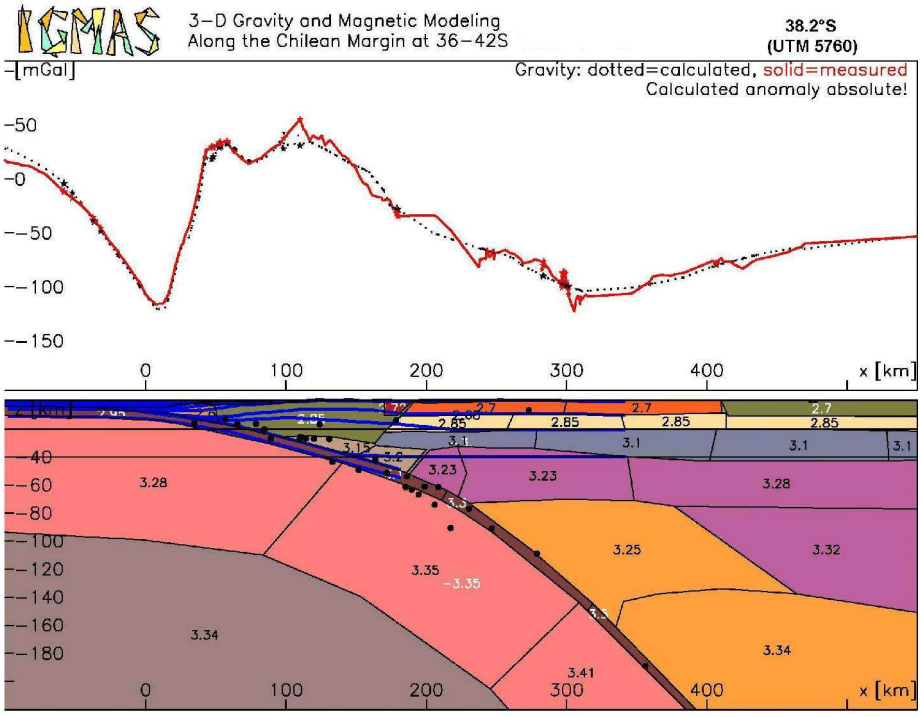

Figure 5.4

A 2D cross section from the density model at ~38.15°S showing model geometry overlain by P-wave velocity boundaries (blue lines) from the SPOC south wide angle reflection/refraction profile and ISSA earthquakes.

Three-dimensional information (gridded surfaces, triangulated models), e.g. isostatic models, 3D crustal balancing, 3D seismic tomography surveys, require three (x, y, z) coordinates and a special topology. These 3D surfaces do not require any projection, they are cut by vertical or horizontal cross sections and visualized by polygon lines.

The interactive modification of model parameters, e.g. geometry and density, access to the numerical modelling process and direct visualization of both calculated and measured fields of gravity, enable an interpreter to design the model as realistically as possible. In this context, a 'realistic' model means that inconsistencies of existing information are kept to a minimum. A basic requirement for modelling is the existence of ideas and hypothesis in a study area, e.g. the availability of quantitative or qualitative constraints. Towards this end, geophysical

modelling aims to combine and compile all existing information. The lack of complete information, which is always the case, has to be overcome by inter- or extrapolation, and contradictions of different data sources have to be clearly identified (Schmidt, 1996) .

The constraining data used to build up the 3D density model of this study are described in Chapter 4. During modelling, all of these data were incorporated digitally in IGMAS. The GIS functions of IGMAS enable an exact projection of the available data onto the modelled structures and avoids any uncertainties that may result from using only approximate overlays and comparison of various datasets.

5.1.4 The reference model

The measured gravity is influenced by the mass of the entire Earth, whereas in the simple density models only a part of the Earth is being considered (e.g. the upper 10 or 100's of kilometers.) Hence the modelled space does not include all the masses below and around the measurement points. This causes an offset of the levels of the measured and modelled values. The offset between the measured and modelled values could be eliminated by modelling the entire mass of the Earth, but this is not realistic.

The modelled gravity field of the study area where the influence of the surrounding areas is not considered will, however, still have the same amplitude variations as the observed gravity (assuming that the surrounding density inhomogeneities have the same effect on the gravity measured on all the points). In any case, it will contain a constant shift from the measured field. This offset can be removed, nevertheless, by introducing a reference model in the background of the density model (Kirchner, 1997). The densities are then modelled relative to this reference model. The reference model has only a few layers but extends to the same depth as the real 3D model and its density values are negative (Figure 5.5).

The selected reference model is constrained by the worldwide compilation of Christensen and Mooney (1995). Their study consists of 560 individual velocity-depth functions. Only the results of seismic refraction/wide-angle reflection have been used. The weighted average crustal thickness based on these values is 41 km ±6.2 km. The crustal density in the reference model for this study has densities of 2.66 g/cm^3 at the surface and 3.1 g/cm^3 at the base of the crust at a depth of 40km. The mean crustal density for this model is 2.835 g/cm^3.

Another study (Rudnick & Fountain, 1995), where seismic data were combined with petrological and geochemical data, shows an even more detailed subdivision of the crust. There are 9 types of continental crust defined, all with 3 layers of crust with typical values of seismic velocities linked to the types of rocks that characterize the layers. The layering typical of Shields/Platforms and Arcs was chosen for the background reference model.

For the lower mantle boundary, PREM 1981 (Dziewonski & Anderson, 1981) was used, where the upper mantle I is a layer defined between 24,4 km and 220 km depth. The maximum depth of the density model is 300 km depth, allowing more of the anomalous mass of the subducting slab to be included.

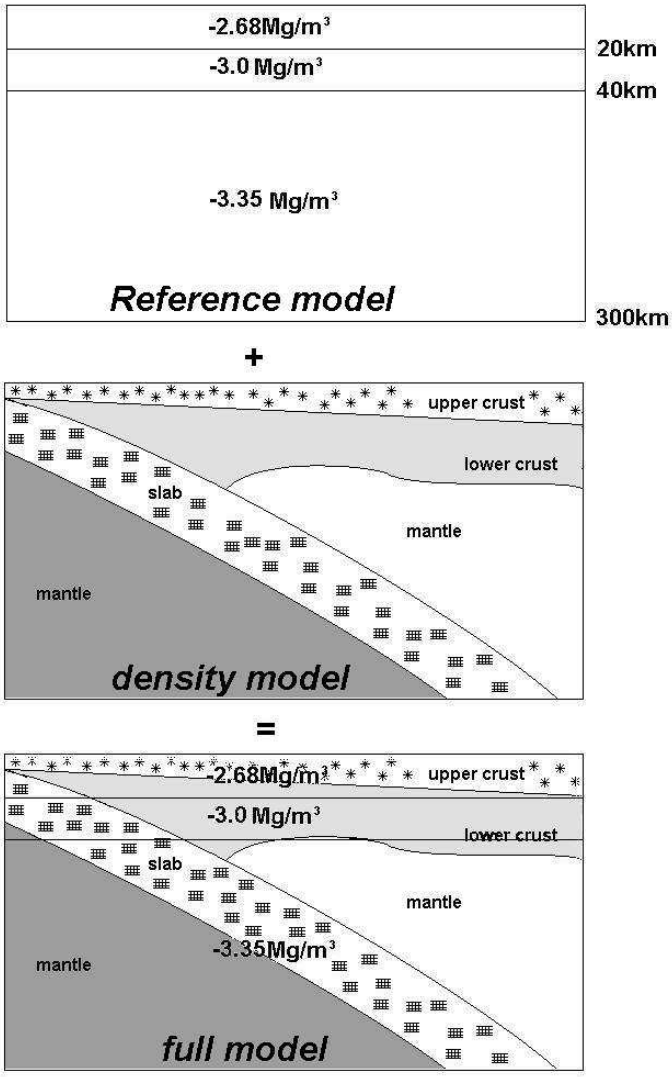

Figure 5.5
The reference model used to calculate the background gravity field for the density model; the average crustal density of 2,84 Mg/m^3 used in the chosen reference model is consistent with the value of Christensen & Mooney (1995).

5.2 Description of the density model

The 3D density model was first developed on 16 parallel east-west cross sections, and was later extended to 28 planes. The first cross section lies at 36.3°S (5980 km in the UTM projection, Figure 5.6), but due to the irregular station distribution (Figure 3.2) the first five planes lie in an area with almost no gravity stations in the forearc (Figure 5.6). The first profile with a good gravity data coverage is at 37°S. The model ends at ~41.7°S (5370 in UTM km). The distance between the planes is 20 km in the northern part of the working area (36°S-40°S) where other geophysical measurements are concentrated. South of 40°S, the spacing between the cross sections is 30 km (Figure 5.6.)

Figure 5.6 (opposite)
The measured gravity anomaly (Free Air offshore and Bouguer onshore) on the left side and the gravity field reproduced by the 3D model on the right side. The horizontal lines represent the 28 2D cross sections that make-up the 3D model. UTM coordinates in km are shown. Small black dots mark the gravity stations; the black dashed lines offshore denote (from left to right) the major oceanic fracture zones (Mocha north and Agassiz' FZ south of it), the trench and the continental slope boundary; and the dashed line onshore marks the position of the Longitudinal Valley. The red triangles denote the volcanoes aligned along the LOFZ. The white lines mark the boundaries of forearc segments discussed in the text. The thick red line marks the position where the subducted slab reduces its thickness and density, as well as age and origin.

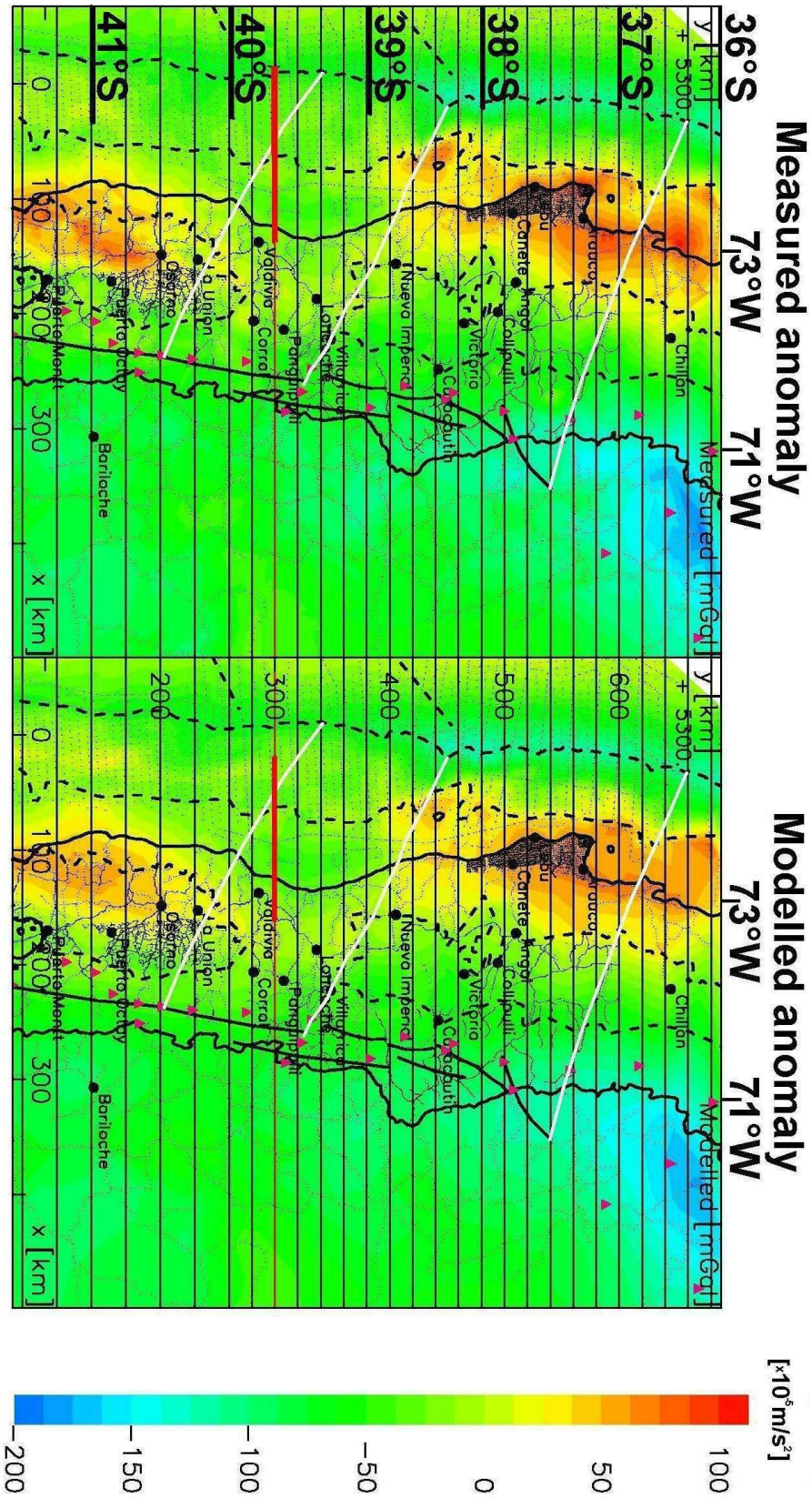
Measured anomaly
Modelled anomaly
36°S
37°S
38°S
39°S
40°S
41°S
73°W
71°W
Measured [mGal]
Modelled [mGal]
y [km]
x [km]
Chillán
Angol
Victoria
Valdivia
Barilache
[×10⁻⁵m/s²]
100
50
0
−50
−100
−150
−200

The density model was built up according to a geological model (Echtler, pers. comm., 2002, Figure 5.7) following the hypothesis that the two positive gravity highs in the Bouguer anomaly field (Figure 3.8) have two different sources. In the northern part of the study area (at latitudes between 36°S–39°S), where the active uplift of the Mocha Island and Arauco Peninsula is observed, the gravity high was interpreted to be the result of the basally accreted material below the basement of the Palaeozoic accretionary complex (Figure 5.7 A.). The southern gravity high, which is shifted eastwards (relative to its position in the northern part, Figure 5.6), was explained by the crustal thinning below the Longitudinal Valley (Figure 5.7 C.) due to the extensional origin of this sedimentary basin. The Valdivia area at 39°–40° S with no pronounced gravity high (Figure 5.7 B.) was interpreted as a 'normal situation'. Based on the different features observed both in geology and in the gravity field, three segments, analyzed in the Section 2.4, were defined in the working area (Figure 5.6). Three representative block sections are shown in Figure (5.7).

The forearc Palaeozoic accretionary complex in the Arauco-Lonquimay segment is characterized by the Eastern Series rocks as well as the intrusive granitoids of the Nahuelbuta Mountains (Figure 5.7 A.). These rocks lie next to the rocks of Western Series (green part of the accretionary wedge). Below them (brown body), the accreted material is present. The Valdivia-Liquiñe segment (Figure 5.7 B.) is characterized by the absence of the Longitudinal Valley and the forearc accretionary wedge is dominated only by Western Series rocks. The southernmost Bahía Mansa-Osorno segment is characterized by the same accretionary wedge, but the Longitudinal Valley is again present and with large amounts of sediment infill (~3 km, references see Section 2.4.3). The feature that distinguishes this segment, is the pronounced crustal thinning below the Longitudinal Valley (Figure 5.7 C.).

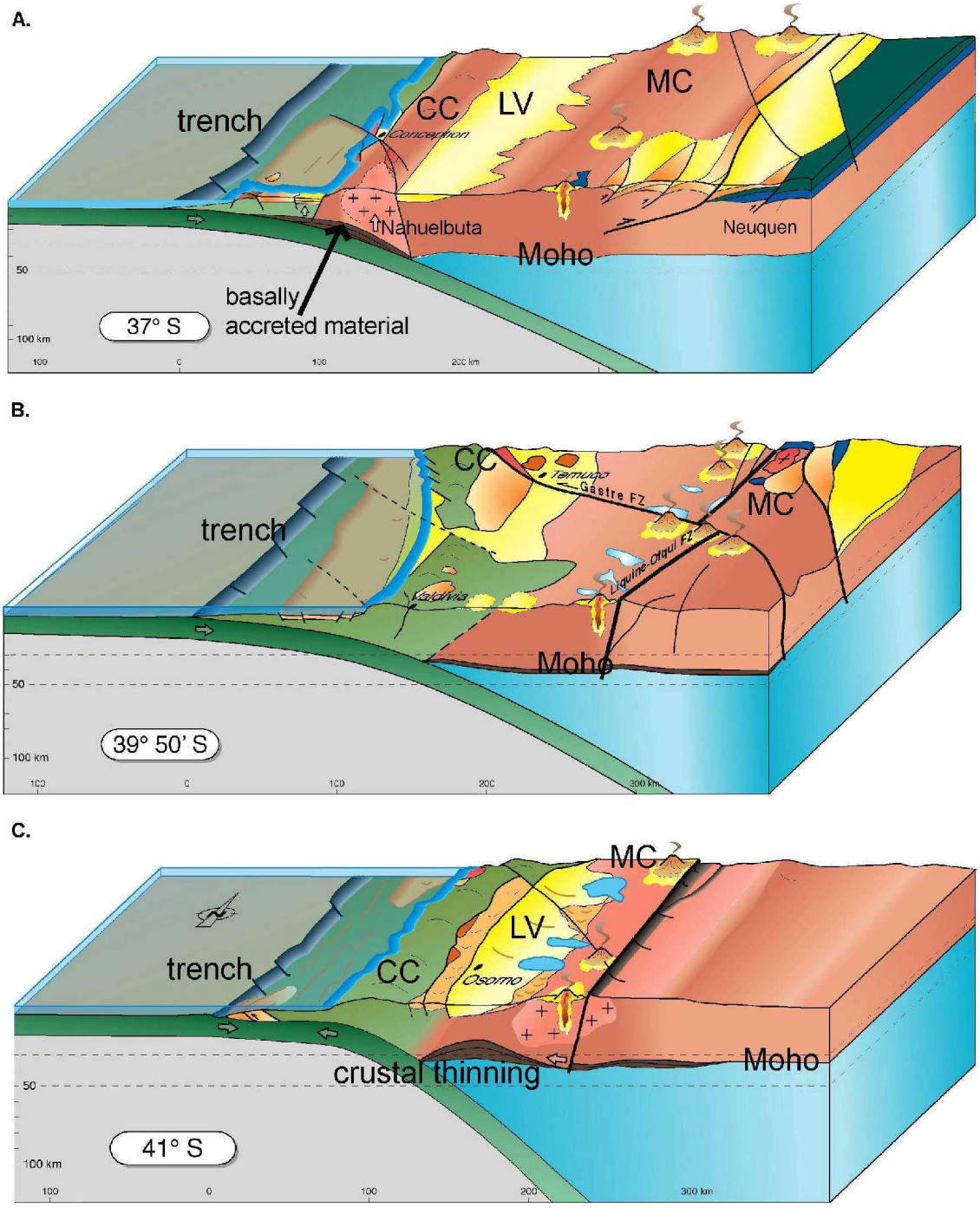

Figure 5.7

Three block diagrams representing the three segments briefly described in Section 2.3. A.) Arauco-Lonquimay (37-39°S); B.) Valdivia-Liquiñe (39-40°S) and C.) Bahía Mansa-Osorno (40-42°S) (Echtler, Melnick, 2002; pers. comm.). The main features are the Western Series rocks of the accretionary prism (green) that represent the Coastal Cordillera (CC). The CC north of ~38°S also includes Eastern Series rocks and granitoids of the Nahuelbuta Mountains (pink,A). The sediments of the Longitudinal Valley (LV) are marked by yellow colour and the active volcanic arc (MC – Main Cordillera) east of LV is also shown.

5.3 The interpretation of the gravity field

The density model developed in this work, as mentioned above, is based on a geological model. The initial hypothesis concerning the origin of the possible sources of the gravity anomalies was used, but during modelling, the following results, summarized in the next section, were obtained.

The measured gravity in the Arauco-Lonquimay segment could not be reproduced using the starting hypothesis that suggested the gravity high is caused by basally accreted material underneath the accretionary wedge (5.7.A). The amplitude and wavelength of the observed gravity high is much too large to be caused by relatively small bodies of the basally accreted sedimentary rock of moderate density. Therefore, the initial hypothesis was also tested applying methods for the wavelength analysis of a gravity field, such as the Fast Fourier Transformation (Degro, 1986; Blakely, 1996; Ebbing, 2002).

Three methods are applied:

1.) The upward continuation of the gravity field (Figures 5.8 and 5.9).The continuation of the gravity field is a method for transforming gravity anomalies at one level to other levels. The continuation can be applied upwards or downwards to any chosen level (e.g. from topography to a higher level). Upward continuation functions as a low pass filter and is used as a method for regional field determination. Downward continuation from the surface requires knowledge of the internal mass structure.

2.) The low-pass filter (Figure 5.10). Wavelength filtering (low-or high-pass) of potential fields is a method that allows the different components of the field to be analyzed. A low-pass filter gives insight into regional features by removing short wavelengths, hence eliminating the effect of local anomaly sources. A high-pass filter removes long-wavelength features showing the effect of local structures.

3.) The isostatic regional/residual anomaly (Figures 5.11 and 5.12).

The crust/mantle boundary is estimated first, based on the topography of the region, for given parameters, which are: density of water, crust, and mantle, normal crustal thickness, rigidity and a chosen model of local or regional isostasy. The gravity effect of such an isostatically compensated Moho is then estimated (e.g. By using Parker's algorithm, Parker 1972, Lahmeyer 1989) to give a regional isostatic gravity field. The isostatic regional field is then substracted from the observed gravity field

to give an isostatic residual anomaly that might enhance small-scale lithospheric density inhomogeneities. However, the residual anomaly may also reflect the wrong choice of the parameters (Lambeck, 1988). Figure 5.11 the Vening-Meinesz regional isostasy model computed assuming a normal crust of 35 km thickness, rigidity of 10^{23}Nm, a density contrast of 0.35 Mg/m^3 at the crust/mantle boundary and the GTOPO30 DEM for the topography (Schmidt, pers. comm., 2003). The regional isostatic field is similar to the FFT and filtered regional fields, as has been shown previously by Wienecke (2002).

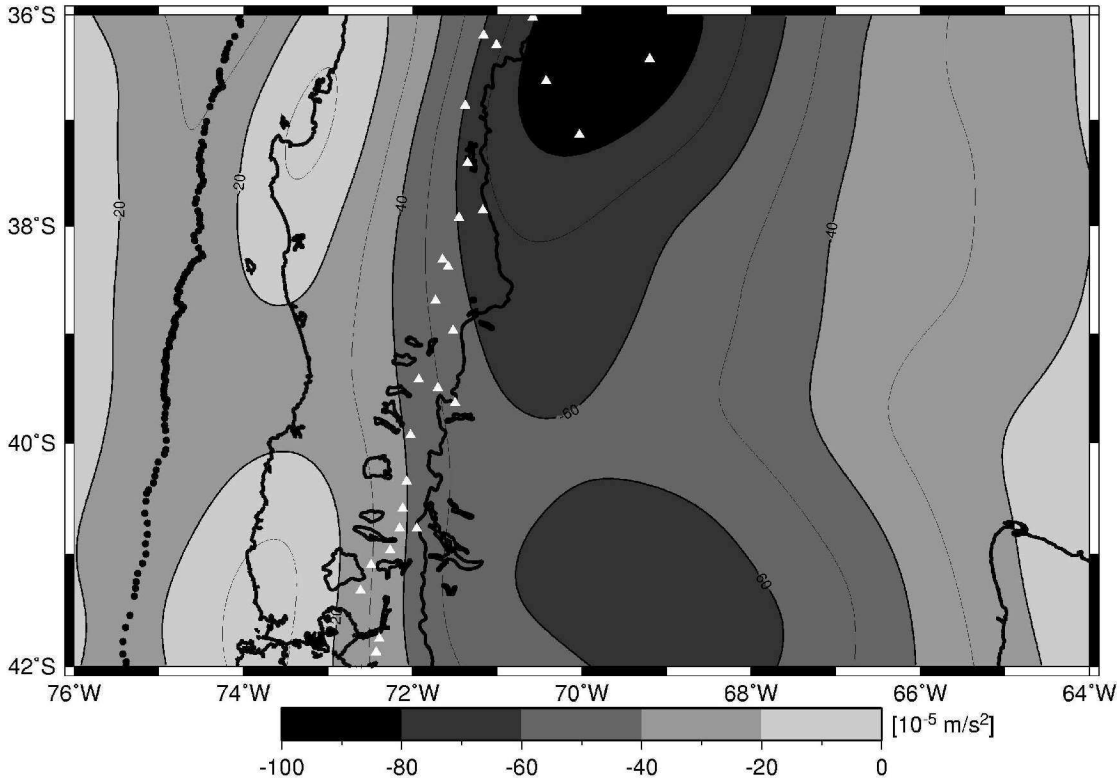

Figure 5.8
The measured gravity field upward continued to 75 km.

A.

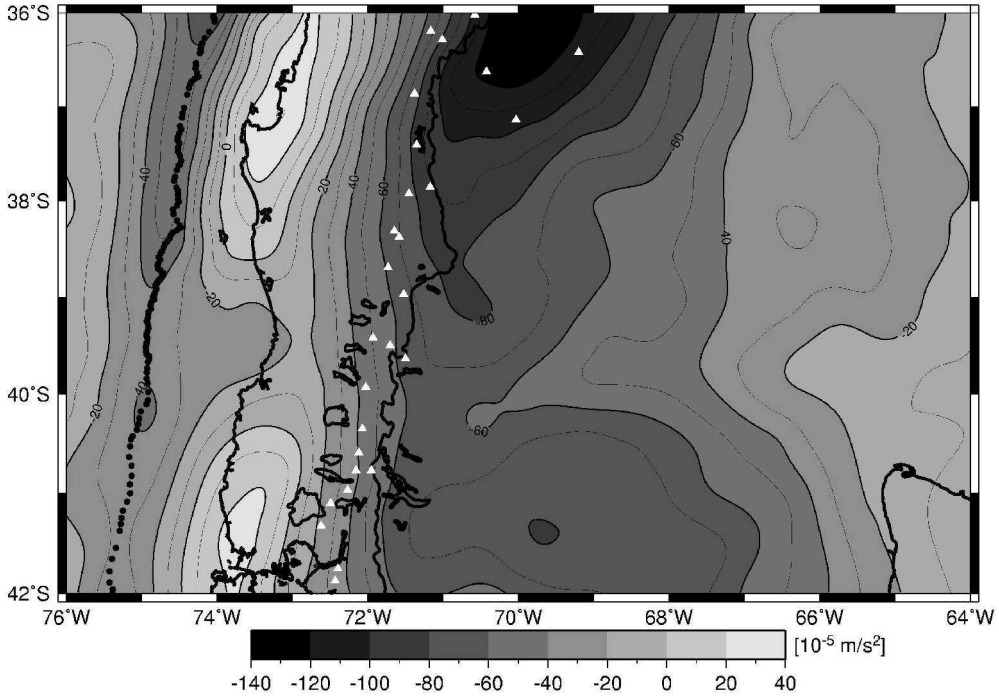

B.

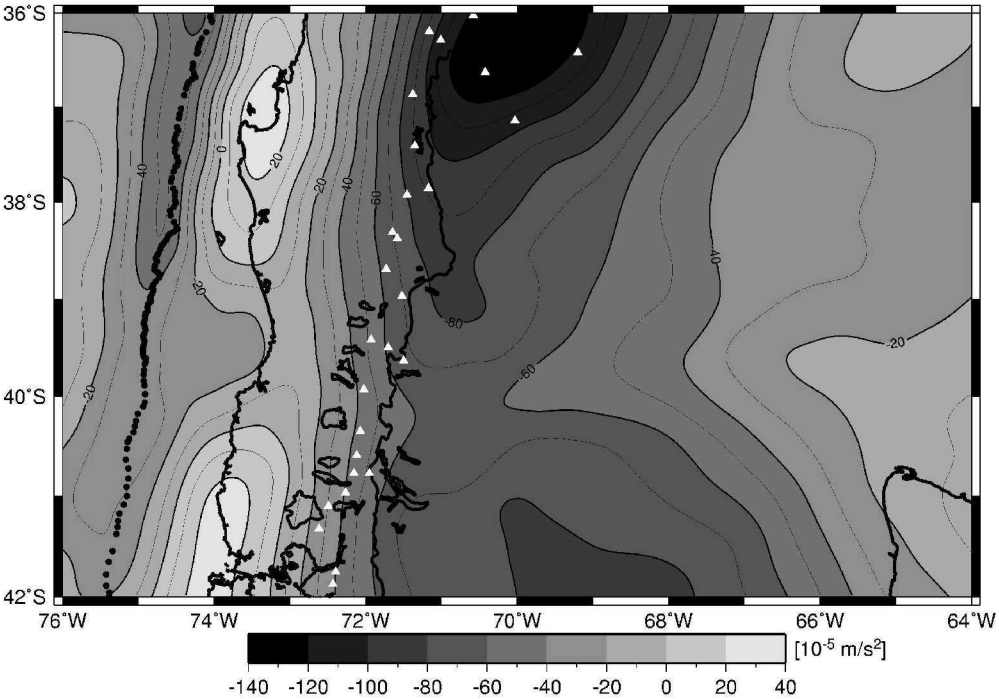

Figure 5.9
(A) measured gravity upward continued to an elevation of 25 km using FFT. (B) gravity predicted from the 3D density model, also upward continued to an elevation of 25 km using FFT.

As seen in the previous examples, the two gravity highs in the forearc, separated by a gravity low in the Valdivia region, and a negative anomaly associated with the main arc (specially at 36–38°S), are ubiquitous features. They must be caused by large structures because they effect the long wavelength part of the gravity field. The images with the results of the low-pass filter and the isostatic regional field (Figures 5.10–5.12), show a similar result. For the low-pass filter, a cut-off wavelength of 400 km was applied (Wavelengths less than 200 km had little effect on the gravity field, indicating that the gravity field's true form is caused mainly by regional features, while local features may also reflect measurement errors).

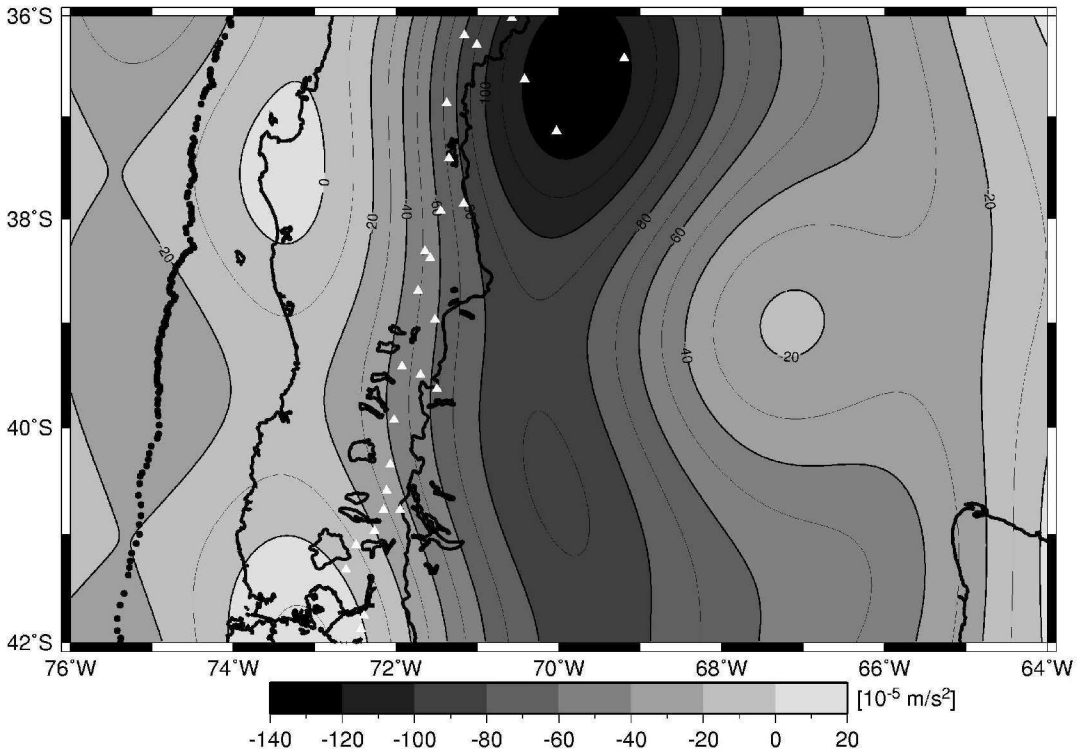

Figure 5.10
Low-passed filtered measured gravity data. The gravity high in the forearc is still partly present after eliminating the effect of features with wavelengths of 0–400 km. The observed gravity minimum below the arc at ~37°S is also preserved.

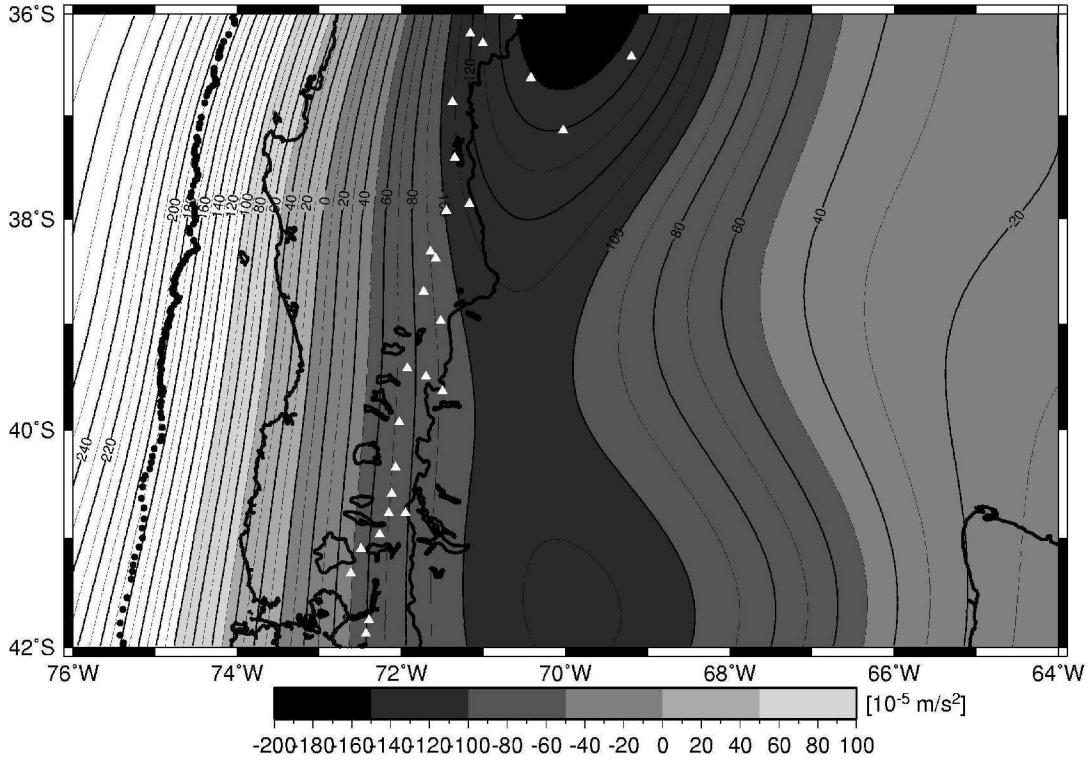

Figure 5.11
The isostatic regional field assuming a regional isostasy model (Vening-Meinesz; 35 km thick crust, rigidity of 10^{23}Nm, a density contrast of 0.35 Mg/m^3 at the crust/mantle boundary and the GTOPO30 DEM for the topography). Positive values are observed in the forearc and negative values characterize the arc.

The remaining isostatic residual field is shown in Figure 5.12. An interesting feature observed is the positive anomaly south of the Neuquén basin. The negative values in this residual field are associated with the trench and the offshore forearc in the Valdivia-Liquiñe segment, which may be associated with the forearc basin. The volcanic arc at 36-37°S is characterized by lower values, whereas south of 38° S the residual anomaly is positive. If the parameters and model of isostasy used to derive the isostatic anomalies are correct, positive values within the residual field indicate thinner and/or denser crust than assumed, and negative values thicker and/or less dense values characterizing the crustal structure.

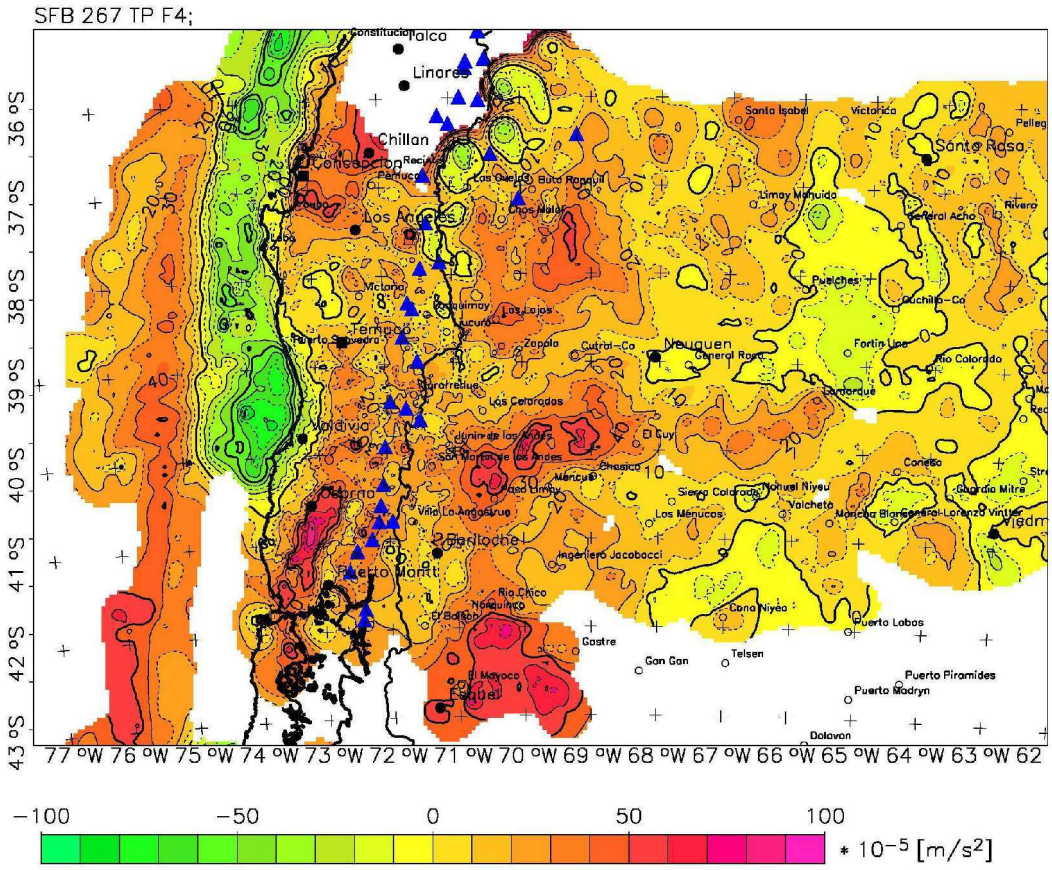

Figure 5.12
The isostatic residual field. The blue triangles mark the volcanic arc. Negative values characterize trench, the continental slope and shelf, the northernmost part of the arc, and partly also the backarc. A positive isostatic anomaly is associated with the forearc, especially in the southern part of the study area (at Osorno), as well as in the arc and backarc south of the Neuquén Basin.

The results presented above lead to the conclusion that the gravity field, characterizing the forearc is dominantly caused by regional features.

The gravity high in the Arauco-Lonquimay segment (37–39°S) must be caused by a much more regional structure than the basally accreted material. Also, interpreting the two forearc gravity highs as anomalous and restricted features to the Southern Andes only is misleading. Figure 5.13 shows the Bouguer anomaly onshore, combined with the Free Air anomaly offshore along the South American coast from 10°S till 43°S. As seen in the figure, the positive anomaly is present everywhere, although it differs in its width and amplitude. A feature that is restricted to the Southern Andes is the gravity low (~0×10^{-5}m/s^2) of the Valdivia region separating the regions of positive gravity. Also, the Bouguer anomaly high south of 33°S becomes broader than elsewhere and has an offset south of 40°S, where it is shifted landwards towards the Longitudinal Valley. Therefore, the source of the

positive anomaly in the Bahía Mansa-Osorno segment, as postulated in the initial hypothesis (Section 5.2), and confirmed by the gravity data and the density modelling, is different to that associated with the gravity high in the Arauco-Lonquimay segment at 36–39°S.

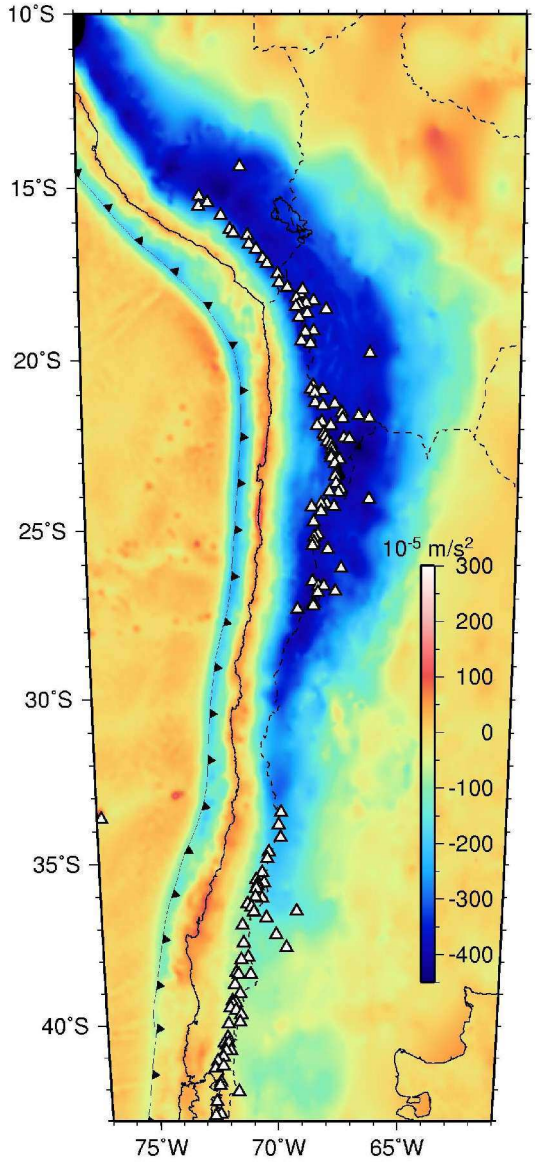

Figure 5.13
Gravity anomalies of the Andean margin. Bouguer anomalies onshore are based on data from Prof. Denizar Blitzkow, Universidade de São Paulo, Escuela Politécnica, Departamento de Engenharia de Transportes, Brazil. Offshore Free air anomalies are based on the KMS 2001 dataset (Andersen and Knudsen, 2001). The volcanic arc is marked by the white triangles and the trench by the black line with triangles. Note the relatively continous positive anomaly along the coastline.

A segmentation similar to that observed within the gravity field, is also observed in the image of the geoid undulation (Figure 5.14). As the geoid is influenced by almost all the anomalous features of the Earth's interior, as well as its topography, it tends to reflect the regional features of the gravity field. Thus, the observed segmentation, correlating well with the differences identified in the Bouguer gravity anomaly, similarly indicate regional features to control the gravity field.

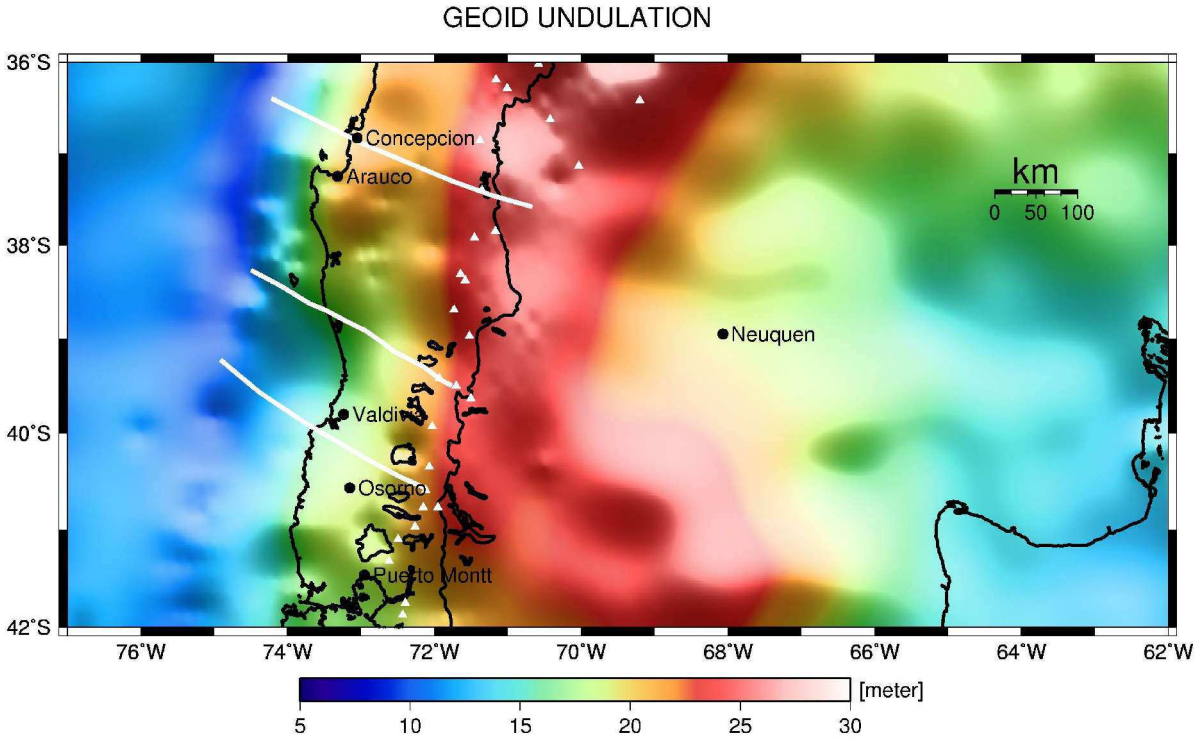

Figure 5.14

The local, high resolution geoid undulation, after Marchenko (2004, in press), overlain by the boundaries of the three segments (white lines) identified in the gravity field and also observed in geology. The Valdivia-Liquiñe segment is characterized by lowest geoid undulation values, the Arauco-Lonquimay segment by highest values. In the Bahía Mansa-Osorno segment, higher geoidal undulation is shifted from the coastline inland.

The following sections describe the resulting geometry and density of the continental and oceanic plates, based on interpretations of the gravity field and forward modelling.

The density model consists of ~40 bodies that represent the following geological units: ocean water, oceanic crust and lithospheric mantle of the subducting slab, continental crust and the asthenospheric mantle (Figure 5.15).

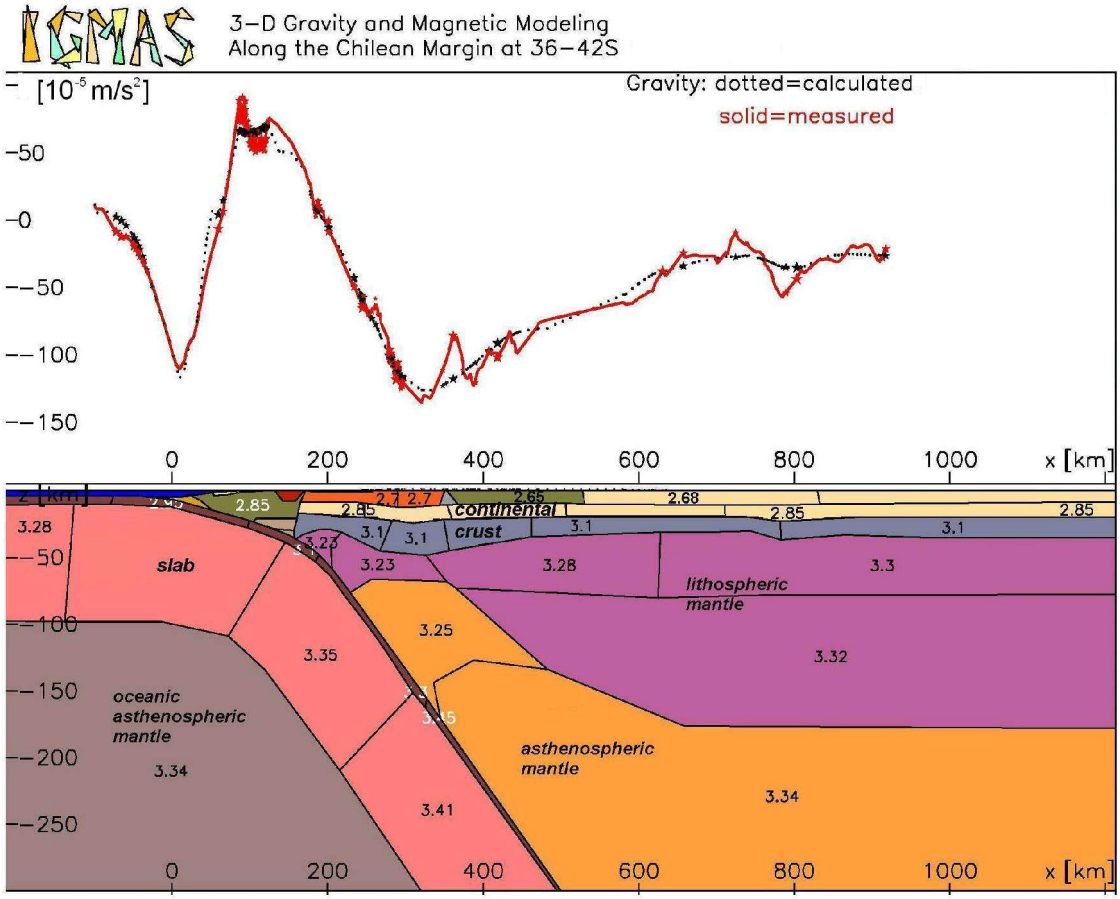

Figure 5.15
A representative 2D cross section from the density model. The upper part of the image shows the measured gravity values (red) and the modelled gravity curve (black dots). The lower part shows the structures of the density model; from left to right: ocean water (blue); oceanic crust (thin brown layer); the continental crust (three layers, with the crust/mantle boundary at the transition of the gray and lilac bodies, where the gray layer represents the lower crust and the lilac the lithospheric mantle); the mantle lithosphere of the slab (pink); asthenospheric mantle (oceanic and continental). The numbers mark the densities of the bodies (in Mg/m^3) and the lines mark their boundaries. The coordinates (UTM projection) as well as the depth are in kilometers.

5.4 The continental plate

5.4.1 Structures and density of the upper plate

The continental crust (apart from that part associated with the accretionary wedge) is represented by three layers. It is constrained based on geological observations (upper crust) and the deeper parts by the velocity models (SPOC and ISSA) and the local earthquake tomography model.

The P-wave velocities listed in the Table 4.1 that were converted to densities (Table 4.2 and 4.3) were used to define the densities of the middle and lower crust. These densities were set to be constant, and have values of 2.85 and 3.1 Mg/m^3 (corresponding to the average velocities of 6.5 km/s and 7.0 km/s for the middle and lower crust respectively). As shown in Table 4.3, these velocity and density values would correspond to a middle crust composed of diorite and a mafic (gabbroic) lower crust. The middle and lower crustal layers have a few separated blocks that allow the lateral density changes to be modelled. In order to keep the model simple and comparable (in terms of composition and crustal thickness), the lateral changes of the middle and lower crust were not modelled and the layers were defined to be homogeneous within the entire model.

The upper crust includes some along strike and lateral changes, constrained by surface geology. The modelled upper crust represents the morphological units shown in Figures 2.5 and Figure 5.16. To model along-strike changes, the crust was divided into three parts, northern, middle and southern. The divisions correspond to changes observed within the volcanic arc and the backarc. The volcanic arc (Principal Cordillera, in orange color Figure 5.16) is divided at 38.5°S and 40°S by a southward increase of density from 2.7 to 2.8 Mg/m^3, representing the more mafic composition of the rocks south of 38.5°S (Cingolani et al. 1991; Section 2.3.4). The green body (Figure 5.16) in the backarc area represents the Neuquén basin, which in reality contains a several kilometer thick layer of sediments. This sedimentary unit was not modelled, but it was considered in terms of a lower density (2.65 Mg/m^3) for the entire body of the Neuquén basin.

The foreland in the backarc region, as well as the North Patagonian massif, are characterized by an upper crust of ~10 km thickness with a constant density of 2.68 Mg/m^3 (corresponding to the density of granitoids, of which the massif is composed, Section 2.3.4). However this region, in therms of crustal structures, is

unconstrained. The Longitudinal Valley was modelled as a sedimentary basin, whose sediment infill locally exceeds 3 km (Jordan et al. 2001), Section 2.3.4. The bulk density used for this unit is 2.6 Mg/m^3, but is not well constrained. The value should, however, represent deep seated sediments as well as the volcanic rocks present within the Longitudinal Valley between 36°S–39°S (Jordan et al., 2001). The thickness of the sediments in the Longitudinal Valley, based on the gravity model, is shown in Figure 5.17.

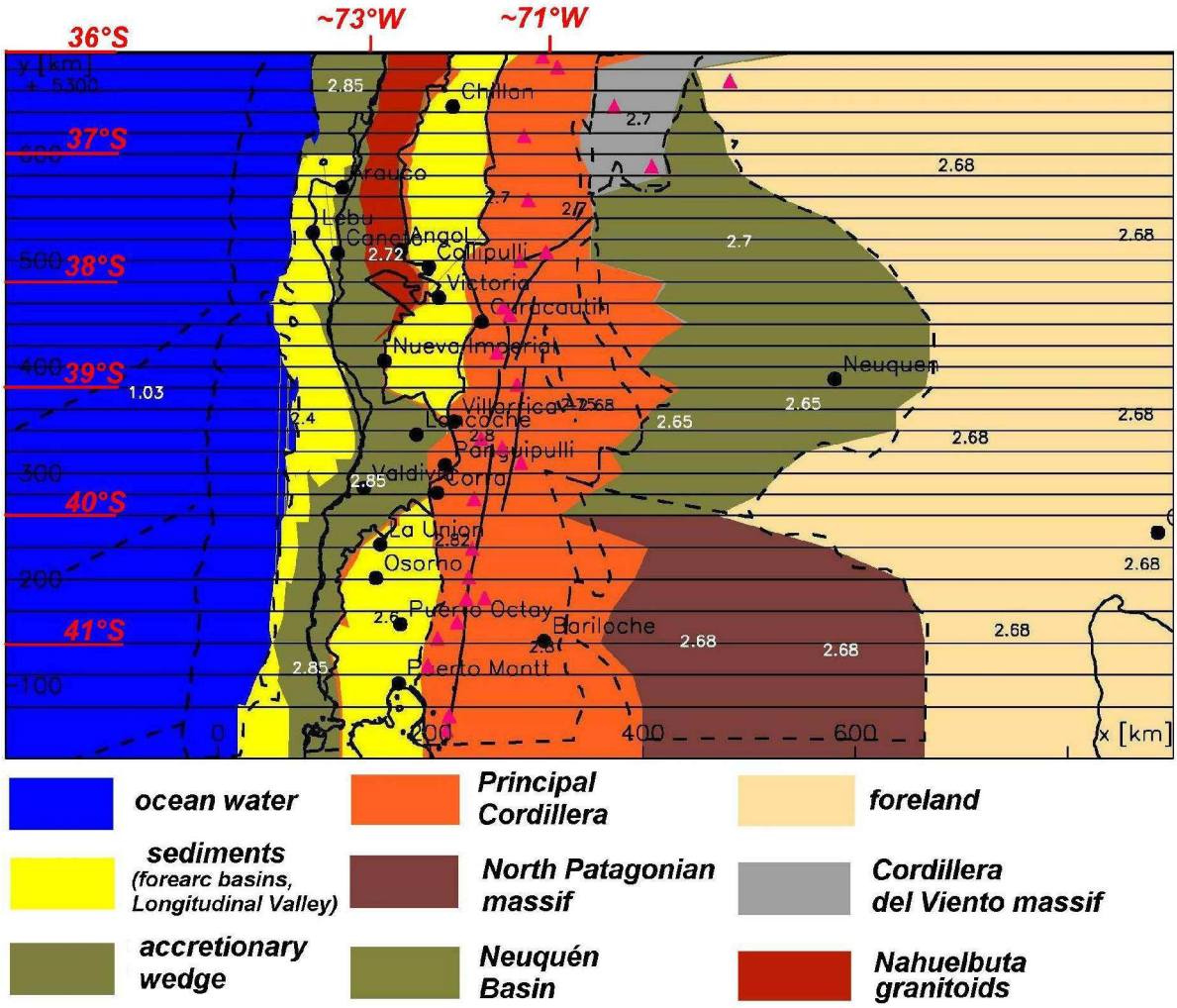

Figure 5.16
A horizontal section through the density model at 0.5 km depth, showing the correlation between near surfaces model geometry (colours) and morphological boundaries mapped at the surface (dashed and solid lines from Figure 2.5). Some of the bodies do not exactly follow the morphological units borders because they were adjusted to the observed gravity (especially those where a large density contrast exists, e.g. Neuquén Basin and the Main Cordillera).

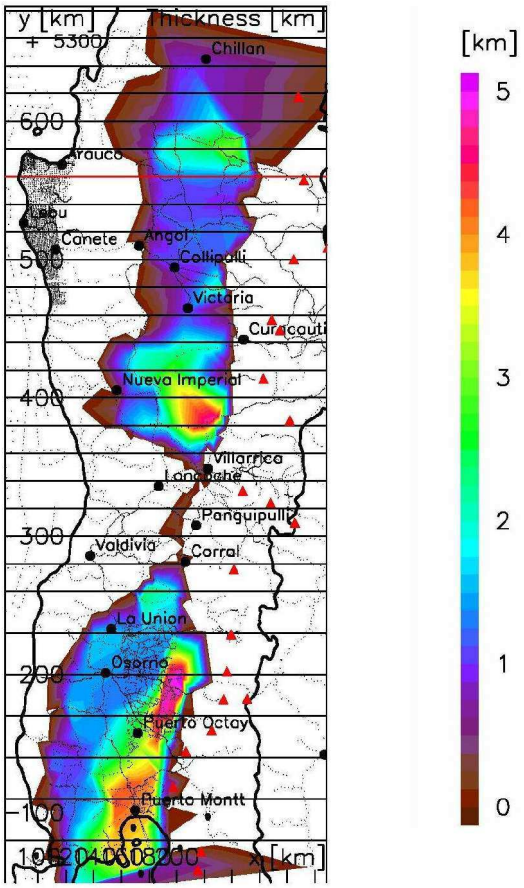

Figure 5.17
Thickness of the sediments of the Longitudinal Valley as it is modelled in the density model in order to match the observed gravity field.

The part of the continental crust closest to the trench represents the Palaeozoic accretionary wedge (Figure 5.18). A density of 2.85 Mg/m^3 represents the rocks of the Western and Eastern Series (Section 2.3.4), whose densities were also measured (Table 4.4). This value remains constant along the entire forearc, reflecting the fact that compositional change does not have any major effect on the bulk density, and should be more or less the same within the working area limits. Western Series high P/T rocks (metabasites, metapelites, metapsammites) also include metasediments and serpentinites, whereas the low P/T Eastern Series rocks (metapelites, metapsammites) do not contain serpentinites. The northern part of the accretionary wedge includes more metasediments than the part south of 38.5°S (Glodny, 2002), and thus the density of this northern part of the accretionary wedge could be slightly lower than the southern part. In terms of the density modelling, such a change is not observed. The forearc north of 38.5°S, due to the pronounced gravity high, requires even higher densities than the values assumed based on the density measurements (Table 4.4) (on average 2.75–2.8 Mg/m^3, depending on the content of the low density sediments). Therefore, the assigned

density value of 2.85 Mg/m^3 follows the seismic velocities, and the gravity data. The SPOC and ISSA profiles are all concentrated in the northern part of the accretionary prism, and none of them shows a constant low velocity feature within the forearc. These profiles constrain also the depths of the slab. Hence, with a geometry of the subducting plate, such as it has been imaged by the seismic data, the pronounced positive Bouguer anomaly can not be explained by a low density accretionary prism (figures in Section 6.3.2). The bulk density of 2.85 has been used along the entire length of the observed accretionary prism, although, south of 39°S, a density of 2.8 is also suitable to reproduce the measured gravity field. A density variation along the coastline, where a less dense accretionary prism would be modelled south of 39°S, would be, however, contrary to the changes observed in geology.

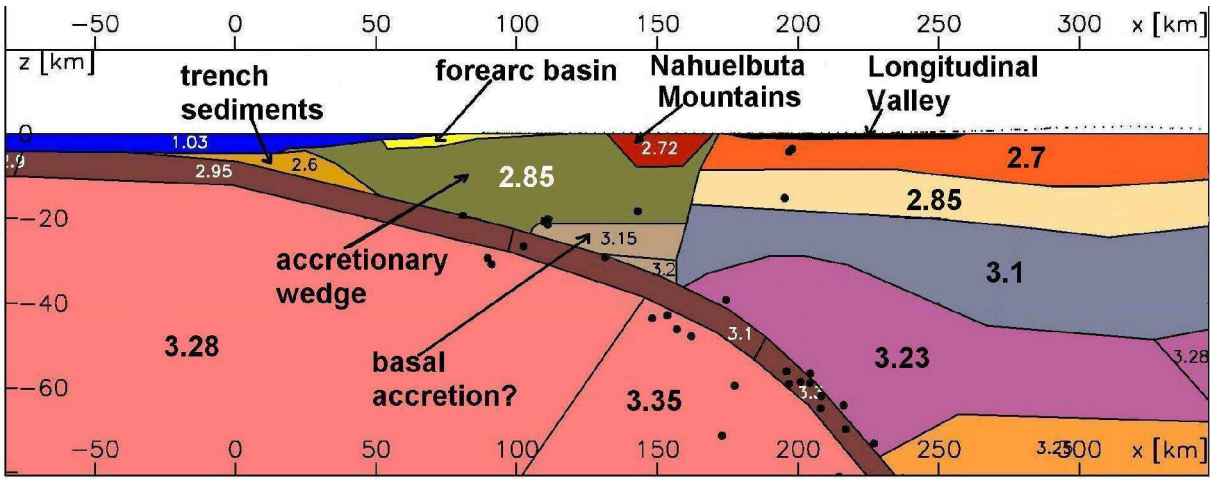

Figure 5.18
The forearc geometry in more detail. The geometry of the slab is constrained from the SPOC and ISSA velocity models, as well as seismicity (black dots) from the ISSA experiment. The crustal thinning below the Longitudinal Valley is inferred from the local earthquake tomography model.

North of 38.5°S the accretionary wedge includes the granitoids of the Nahuelbuta Mountains, characterized by a lower density (2.72 Mg/m^3, Table 4.4). This part of the accretionary wedge should also include a small component of mafic rocks underlying the granitoids, as well as part of the Eastern Series rocks westwards of the Nahuelbuta. The Eastern Series should lie between the Western Series rocks outcropping at the coastline and the granites. Because the Eastern Series form only a smaller body composed of rocks of a similar composition, for simplicity they are not included within the density model. Everything below and next to the Nahuelbuta Mountains was modelled as one body (Western Series rocks),

apart from a high density body at the base of the accretionary prism. This body represents the basally accreted material interpreted by Echtler (2002, pers. comm.) to be causing the uplift of this region, as well as the gravity high above it. This body will be discussed in more detail in Chapter 6.

5.4.2 Thickness of the continental crust

As described in the previous section, the crust has been divided into upper, middle and lower crustal layers. Based on the final density model, the continental crust is on average 40-45 km thick, with local extremes of 54 km and 23 km thickness (Figure 5.19).

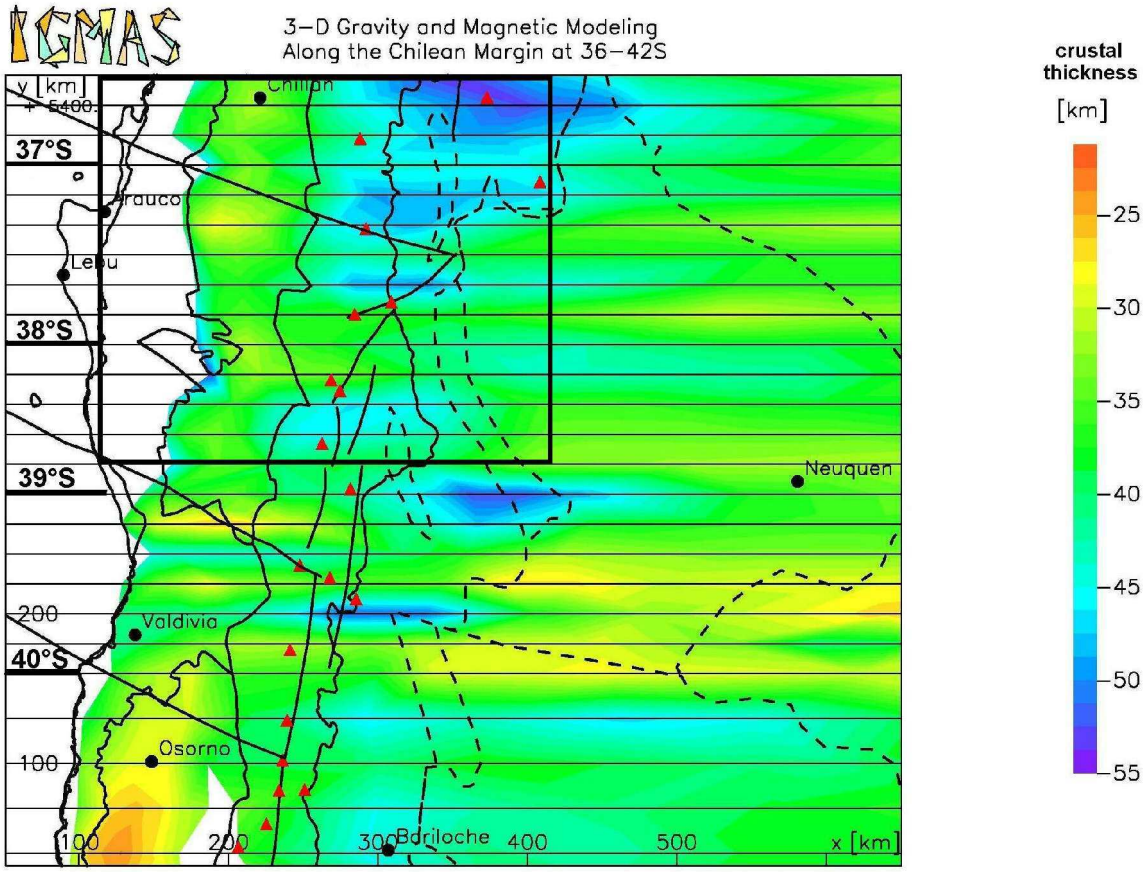

Figure 5.19
The modelled area with all 28 vertical planes (black lines), the three segments (black oblique lines), with an overlay of the morphological units (from left to right: Coastal Cordillera, Longitudinal Valley, Main Cordillera with volcanic arc (red triangles), and in the backarc the Neuquén basin and the North Patagonian massif (Figures 2.5 and 5.16). The black box markes the location of the local earthquake tomography model. There the results (Bohm, 2004) show crustal depth of ~40 km below the forearc and 50-55 km below the arc. These depths beneath the arc are only interpreted in the gravity model below the arc at ~36.5°S where the Bouguer gravity field reaches values of -180×10^{-5} m/s^2. The arc between 37–39°S has an average crustal thickness of ~45 km, whereas south of 40°S it decreases to 35–40 km.

5.4.3 The upper and middle crustal layers

Based on the final density model, the average thickness of the upper crust is 10 km, with the thinnest crust (8 km) occurring east of the Main Cordillera (~38-40° S), and the thickest (15 km) at the volcanic arc (~36.5°S). The assigned densities used in the modelling correspond to the material of the morphological units defined within the study area (Figures 2.5 and 5.16).

The thickness of the middle crust ranges from 15 to 25 km, with an average thickness of 10 km. Based on the P-wave velocities of the SPOC and ISSA models and density-velocity conversion, its density is 2.85 Mg/m^3 (Tables 4.1 and 4.2). The middle crust is thinnest at the forearc along two profiles at 36.6°S and 40.6°S. Thus, the resulting relatively shallow and dense material of the lower crust contributes to the positive Bouguer anomaly in this region. The maximum middle-crustal thickness occurs at the volcanic arc (~36.5°S), where the values of the average Bouguer anomaly reach ~ -150×10^{-5} m/s^2. Hence, the thicker middle crust contributes to the mass deficit necessary to match the observed gravity field.

The crust, upper, middle and lower, is thickest at the volcanic arc. If the upper and middle crustal layers at ~36.5°S were modelled with an average thickness of only 10 km, the mass excess would have to be compensated by a thicker lower crust (up to 60 km).

5.4.4 The lower crust

The only additional geophysical data that constraints the continental Moho is based on the receiver function study (Yuan et al., 2004, submitted). These results (in Section 4.2.1) show the Moho at 40 km depth below the main arc, with a crustal thinning to about 35 km east of it, and ~20 km below the coast (Figure 4.5). This profile, together with P-wave velocities from the seismic profiles converted to densities, was used to determine the density of the lower crust that would best match the gravity field. The derived density of the lower crust in the final density model is 3.1 Mg/m^3 and is kept the same throughout the entire model. In reality, heterogeneity is possible, and also expected, but because there is insufficient data, different densities within the lower, as well as the middle crust, were not modelled. Assuming constant lower crustal density simplifies the model.

5.5 The oceanic plate

5.5.1 Density of the subducting slab

Ocean water (blue, Figure 5.15) has a density of 1.03 Mg/m^3 (the anomaly offshore is the Free Air anomaly), and its geometry is constrained by the Zapata bathymetry grid (Zapata, 2001) and SPOC (Reichert & Schreckenberger, 2002). The subducting slab is represented by the oceanic crust (brown) and the lithospheric mantle (pink, Figure 5.15). The entire slab consists of 9 separate blocks to incorporate different density values. The trench sediments and the active frontally accreted sediments are represented by the dark yellow body with a density of 2.6 Mg/m^3.

The *oceanic crust* is modelled as a one layer body with a constant density value and a thickness of ~7 km (Lüth et al., 2004). In reality however, it is composed of an upper layer of sediments, a layer of mid-ocean ridge basalt (MORB), and a lower gabbroic layer. All of these layers are represented in the model by the bulk density of 2.9 Mg/m^3 at the beginning of the subduction before the plate enters the trench, increasing to 3.5 Mg/m^3 at depths of 200–300km. This density change represents the mineralogical reactions occurring within the oceanic crust with changing P/T conditions. These reactions include the dehydration (fluid release), since the oceanic crust carries an abundant water supply into the subduction zone. The hydrous basalt and gabbro convert to blueschist at relatively low pressures (representing 30 km depth) (Stern, 2002). At greater depths, the oceanic crust progresses through the blueschist –> eclogite, or greenschist –> amphibolite -> granulite -> eclogite facies, depending on the shear heating. For oceanic crust containing 1-2 wt% H_2O, dehydration will not begin until the onset of eclogite- or amphibolite-facies metamorphism, depending on the *P-T* path (Peacock, 1993). Large amounts of H_2O released by blueschist -> eclogite dehydration reactions could trigger partial melting in the overlying mantle wedge and may play a crucial role in the generation of arc magmas (Peacock, 1993).

In detail, the densities used in the 3D model for the oceanic crust, based on the Hacker et al. (2004) approach, are as follows:

- 3.1 Mg/m^3 at depths between 30 and 70 km, similar to the estimated density for blueschist facies rocks,

- 3.3 Mg/m^3 at a depth between 70 and 200 km, representing lawsonite-amphibole eclogite,
- 3.5 Mg/m^3 for depths below 200 km, representative of eclogite facies.

The *mantle lithosphere* is thought to have an upper part consisting of harzburgite and a lower layer of less depleted lherzolite. It is slightly more dense than the underlying asthenosphere, allowing the subduction of the oceanic plate (Stern, 2002). The density of the oceanic lithospheric mantle, as well its thickness, are age dependent. The thickness of the modelled slab mantle is ~90 km in the northern part of the model and decreases to ~50 km south of 40°S, where the slab becomes younger (Section 2.3.1, Figure 2.3). Apart from the plate-thickness difference, there is also a density difference within the plate's lithospheric mantle observed from the modelling results. This change occurs south of 40°S (Figure 5.6) where the density is 0.02 Mg/m^3 less.

The density of the slab mantle increases with depth from 3.28 Mg/m^3 to 3.41Mg/m^3. This change reflects the dehydration and corresponding densification of the slab, for one of the important reactions occurring within the mantle lithosphere is the breakdown of serpentinite into olivine, orthopyroxene and water. The density increase may be large, since this reaction releases a great deal of water. The density values of the slab mantle were estimated using the method of Hacker et al. (2004) (Section 4.3.2).

The SPOC results (Figure 5.20) show that the trench at latitudes 36-40°S is gradually shallowing from 5000 m north of 37°S to 4200 m in the south. It is also becoming broader from ~50 km in the north to ~110 km at ~40°S. The trench is filled with a wedge of sediments increasing in thickness from west to east, which is estimated to be between 1.5 and 2.8 km thick (Reichert & Schreckenberger, 2002).

The bathymetry and the trench geometries are based on the Zapata grid file (Zapata, 2001) and the results of the SPOC (Reichert & Schreckenberger, 2002). The bulk density of the trench sediments, and frontally accreted sediments, is 2.6 Mg/m^3, but this value is not constrained. Nor is the geometry of the frontal accretion unit. Both are based purely on the gravity model (Figure 5.21).

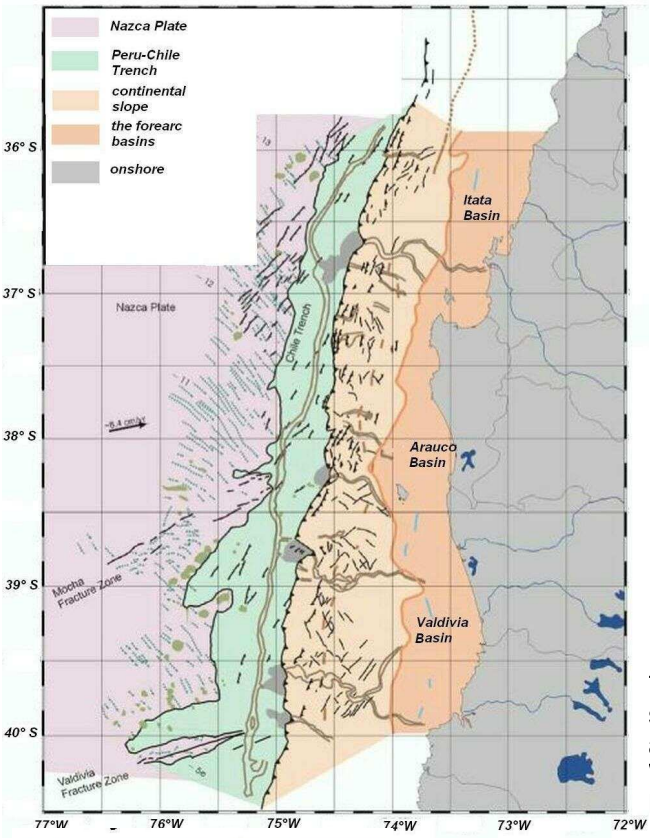

Figure 5.20
The geometries of the trench (trench sediments in green colour), continental slope and the forearc basins (Itata, Arauco, Valdivia) in the study area. Modified after Reichert & Schreckenberger, 2002.

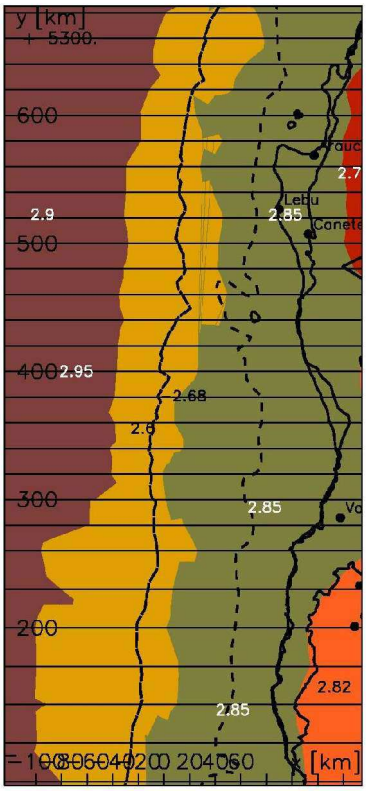

Figure 5.21
The trench sediments (yellow) of the density model at 5 km depth. The trench is denoted by the black line on the left. The trench material landwards of the trench represents active frontal accretion.

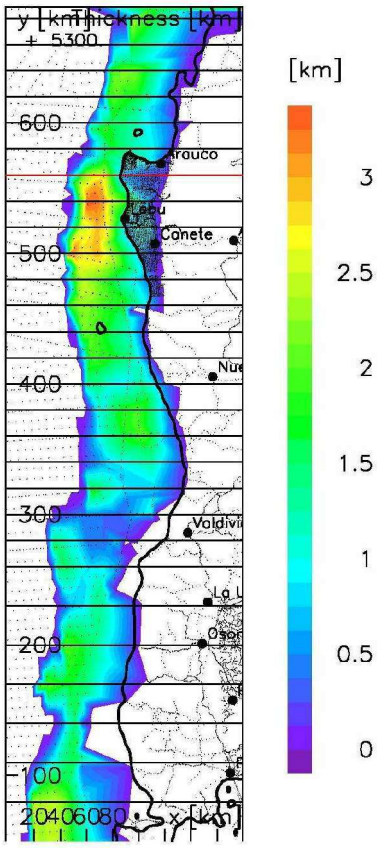

Figure 5.22
The thickness of the offshore basins constrained by the gravity modelling.

Offshore forearc basins are considered within the model and are also necessary to match the observed gravity field. All three basins, Itata, Arauco and Valdivia (Figure 5.20) have been modelled and are characterized by a low density value of 2.4 Mg/m^3. This value is not constrained by any other geophysical data and is based only on the modelling results. The thickness of sediment layer in the basins is shown in Figure 5.22.

5.5.2 Position of the subducting slab

The position of the Nazca plate and its density have a significant impact on the gravity field. With the exception of the Valdivia region, corresponding to the area of the large 1960 Valdivia earthquake, a positive Bouguer anomaly occurs along the South American coastline (Figure 5.13). The gravity field, based on the interpretation of the final density model, is strongly influenced by the depth of the downgoing slab and the material within the continental crust above it. The slab within the model is deeper south of 39°S (Figure 5.23), partly due to the greater distance of the trench from the continent. From 36 to 38°S, the distance of the trench from the coastline is approximately 90 to 100 km, with a minimum distance of 75 km at the Arauco Peninsula (37°S). The coastline then retreats in the Valdivia region (39–40°S) where it reaches a maximum distance of 130–140 km from the trench and the downgoing slab is at its deepest position (36-44 km). South of 40°S, the distance between the coastline and the trench narrows again to about 110 km.

Conversely, the volcanic arc converges southwards to the coastline. The volcanoes south of 39°S lie approximately 230–250 km from the trench, some 30–60 km closer than at 37-38°S. This geometry might also indirectly indicate the position of the oceanic plate below the arc, because according to some interpretations, the volcanoes are usually situated 60–140 km above the slab (England, 2004).

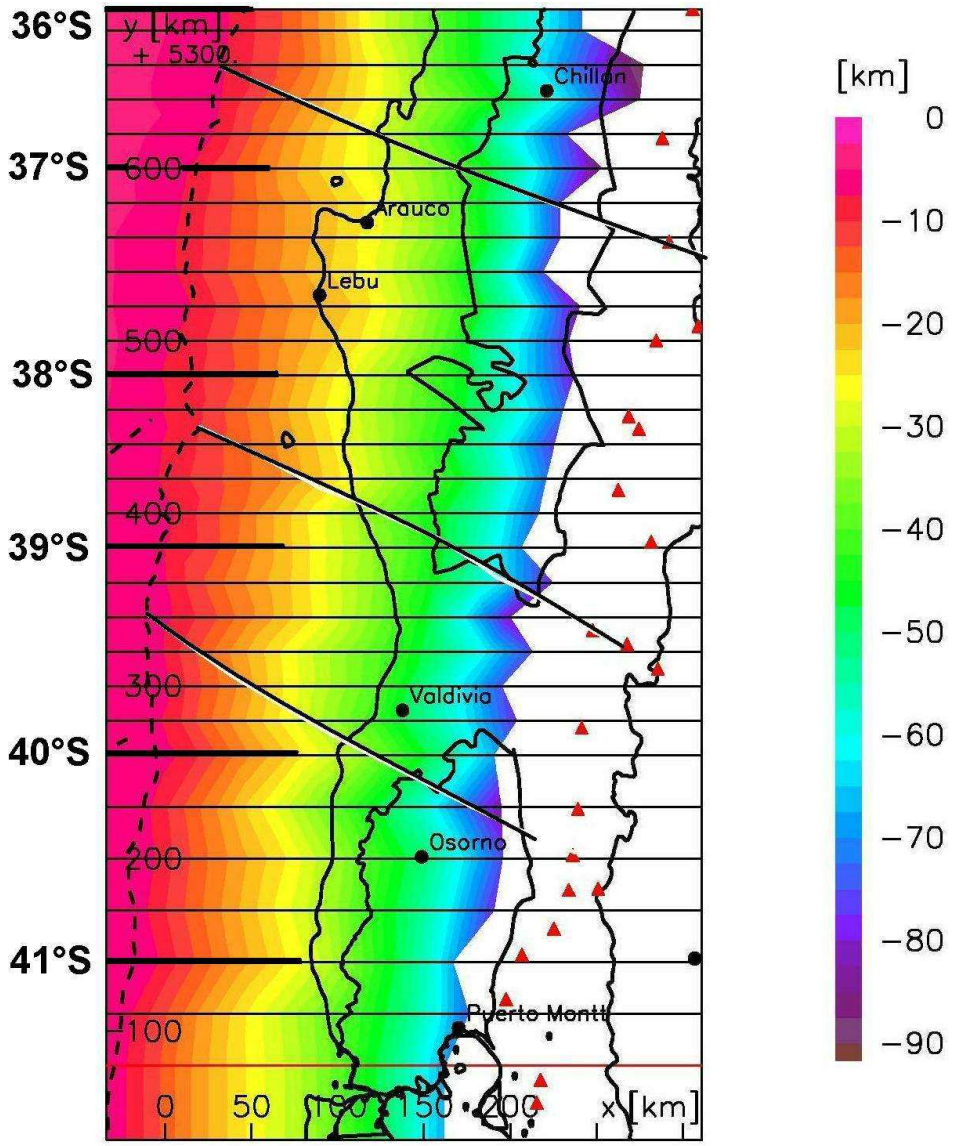

Figure 5.23
The depth of the Nazca plate from the trench (axis indicated by the dashed line on the left side), to the Longitudinal Valley, within the three segments (oblique black lines) of the 3D density model (UTM coordinates in kilometers). The slab is shallowest below the Arauco Peninsula, and deepest below the forearc of the Valdivia-Liquiñe segment, where the coastline is far from the trench.

The different gravity field south of 39°S beneath the forearc is in the density model interpreted to be influenced by the deepening slab. Similar variation of the slab position is observed also in the seismic data, although north of 39°S. The seismic data shows that the slab is deepest at 36.15°S, then it shallows to some 30 km below the coast at 37.2°S and gradually deepens along the SPOC southernmost profile. The geometry of the slab along the ISSA profile at 38.8°S is similar to the SPOC south profile (Figure 5.24).

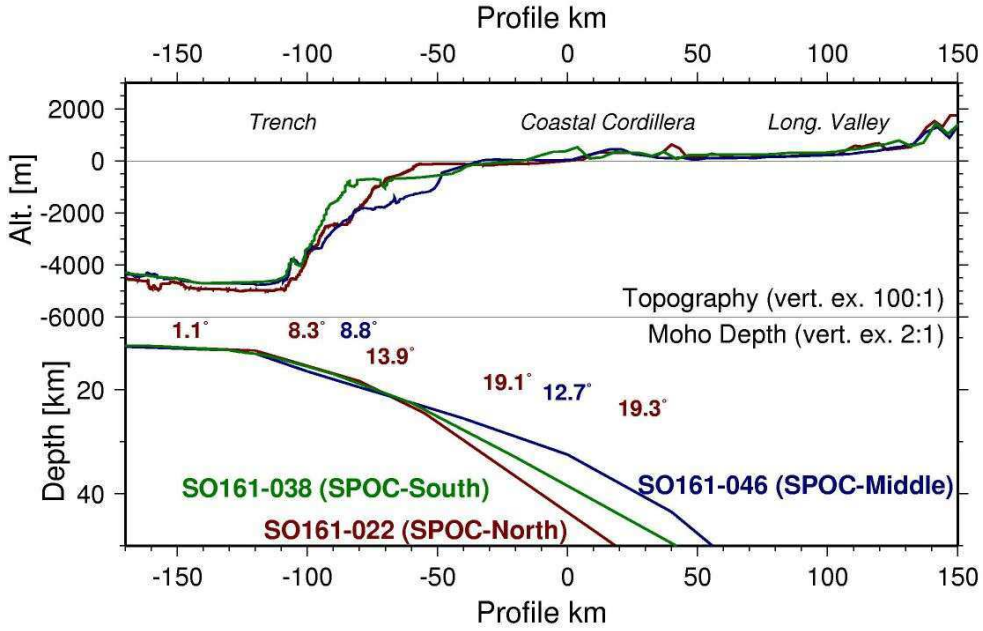

Figure 5.24
The position of the Nazca plate as it has been imaged along the three SPOC velocity profiles (Lüth et al., 2004).

Between approximately 39 and 40°S, where the geometry of the slab is not constrained by any seismic data, the depths of the oceanic plate compared at constant distances of 50, 100 and 130 km away from the trench, show a gradual southward deepening of the slab (Figure 5.25). The depth of the Nazca plate beneath the southernmost Bahía Mansa-Osorno segment is here again slightly shallower than in the Valdivia-Liquiñe segment. Table 5.1 shows the depths of the slab along some profiles in each three segments. The change of the slab depth is more pronounced 100 km from the trench and, in general, it reaches depths below the forearc of 24–29 km in the Arauco-Lonquimay segment, 28–35 km in the Valdivia and 28–32 km in the Bahía Mansa-Osorno segments.

PROFILE ***at latitude***	**Depth [km] 50 km from trench**	**Depth [km] 100 km from trench**	**Depth [km] 130 km from trench**
36.7 °S	-18	-29	-37
37.3 °S	-16	-25	-33
37.8 °S	-16	-24	-33
38.4 °S	-17	-28	-37
38.8 °S	-17	-29	-36,5
39.2 °S	-17	-28	-36
39.4 °S	-18	-31	-39
39.8 °S	-19	-33	-42
40.8 °S	-18	-30	-39
41.3 °S	-19	-32	-40

Table 5.1
The position of the slab below the forearc at distances 50, 100 and 130 km from the trench.

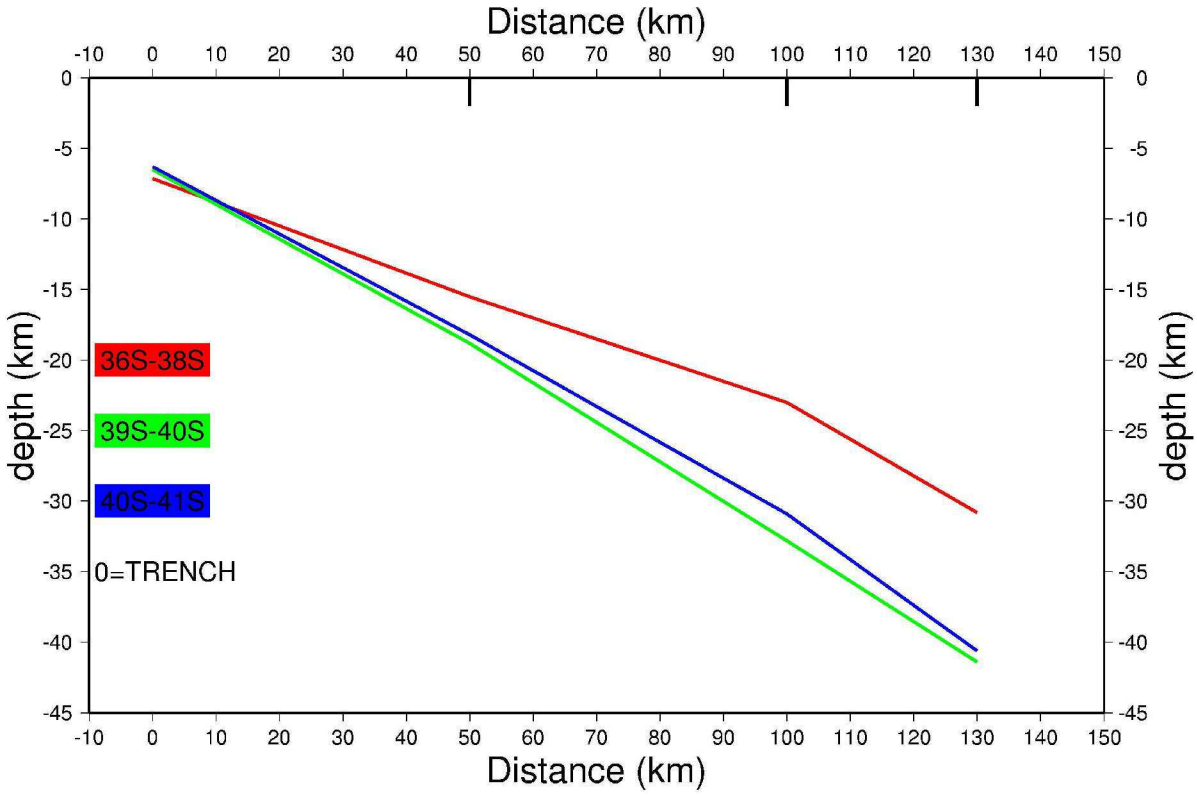

Figure 5.25
The slab dip along selected profiles representative of each of the three segments. The red one corresponds to the profile with minimal depths below the Arauco peninsula, whereas the green one represents the profile with the maximum depths in the Valdivia-Liquiñe segment. The difference in depth 100 km distant from the trench reaches 10 km.

As previously noted, the study area south of 39°S is not constrained by any other geophysical data. Thus, these results of the slab position are only valid assuming that the constant bulk density value of 2.85 Mg/m^3 of the forearc accretionary prism is correct (see Section 5.4.1). With a lower density in the upper plate, the position of the slab can be changed by several kilometers per 0.05 Mg/m^3 density difference. The dependence of the position of the slab on the upper-plate structures will be discussed further in Section (6.3.2).

5.6 Summary of the density model results

The gravity data analysis and modelling, focused on the forearc-arc region of the study area, indicate that the change of the gravity field can be explained by variations in the depth to the slab at the coastline and to the Moho below the Longitudinal Valley and the main arc.

The slab is the shallowest beneath the Arauco-Lonquimay segment (22–31 km). In contrast, the arc is characterized by the greatest depths to the Moho within the study area, reaching a maximum of ~50 km. The Moho depth, however, is shallower beneath the Longitudinal Valley (~35 km) and both Moho features can also be observed in the local earthquake tomography model (Figure A.2 A).

The depth to the slab at the coastline is greatest beneath the Valdivia-Liquiñe segment (36–44 km). In this segment, the depth to the Moho beneath the main arc averages 40 km, as it does below the forearc (at these latitudes the Longitudinal Valley is absent) (Figure A.2 B).

The Bahía Mansa-Osorno segment is characterized by an intermediate slab depth at the coastline (32–36 km). The depth to the Moho beneath the well developed Longitudinal Valley south of 40°S is ~25–30 km depth. This relatively shallow crust/mantle interface is a possible explanation for the positive Bouguer anomaly in this region. The main arc crust is also thinner in this segment than elsewhere, with the Moho generally 35 km deep (Figure A.2 C).